per second at a pressure of about 0.15 MPa in an interval of temperatures up to 500°C.

References

[1]Reymal, L. R., Kapusta, A. B., and Likhachova, A. I., "Magnetohydrodynamic Processes in Devices with Curvilinear Channels," Energoatomizdat, Moscow, 1986.

[2]Kapusta, A. B., Likhachova, A. I., and Mikhailovich, B. M., "Elaboration of Spiral Inductive-Conductive Pump," *Proceedings of the 14th International Riga Conference on MHD*, Inst. of Physics, Riga, Latvia, 1995, p. 65.

[3]Zibold, A. F., Kapusta, A. B., Likhachova, A. I., and Reymal, L. R., "3-D Flow in Screw Channel of Inductive Pump," *Magnitnaya Gidrodinamika*, No. 2, 1986, pp. 121–124.

Chapter 35

Direct Numerical Modeling of Kinematic Dynamo Effect: Application to the French Fast Breeder Reactor Phenix Core's Geometry

F. Plunian,* A. Alemany,† and Ph. Marty‡
Laboratoire des Ecoulements Géophysiques et Industriels, Grenoble, 38041, France
and
Ph. Massé§
Laboratoire de Mécanique et de Génie des Procédés, ENSPG, Grenoble, 38026, France

Nomenclature

$\boldsymbol{A}$ = vector potential, v/s/m^{-1}
$\boldsymbol{B}$ = magnetic induction, T
$\boldsymbol{E}$ = electric field, V/m^{-1}
$\boldsymbol{H}$ = magnetic field strength, A/m^{-1}
Q = flow rate, m^3/s^{-1}
R_m = magnetic Reynolds number
$\boldsymbol{V}$ = velocity field, m/s^{-1}
μ = magnetic permeability, H/m^{-1}
μ_0 = magnetic permeability of free space, H/m^{-1}
σ = electrical conductivity, Ω^{-1}/m^{-1}
φ = electric potential, V

I. Introduction

DYNAMO effect describes the conversion of kinetic energy into magnetic energy by the motion of an electrical conductor medium. This

*BP53X.
†BP 53X.
‡BP 53X.
§Institut des Sciences Nucléaires, 53 ruedes martyrs.

phenomenon permits us to explain the existence of a magnetic field in most of the astrophysical objects, like the sun or the Earth. Without such a mechanism, Earth's magnetic field would have disappeared a long time ago. Besides, the Earth's magnetic field's polarity reversals observed by the paleontologists can find consistent justifications in these mechanisms. They result from the coupling of several physics disciplines, such as thermodynamics (for Earth, the primary source is from the thermic origin), electromagnetism, and fluid mechanics.

In the case of the Earth, the dynamo effect is desirable (Earth magnetic shield); in revanche it is not the case in the large industrial realizations containing liquid sodium.[1] Thus, the fast breeder reactor (FBR) authorities have requested the support of researchers to realize the measurements inside the reactors. Even if some results have shown a semidynamo mechanism correlated to thermoelectrical currents in the first loop of a FBR,[2] no dynamo effect has actually been observed.[3,4] However, one part of the reactor has never been the object of direct electromagnetic measurements: the core of the reactor, which contains the plutonium and the uranium fuel.

We have been requested to carry out a general program concerning the analysis of the different possible sources of the magnetic field inside the first sodium loop of the French reactor Phenix. Several analytical results have already been found.[5,6] The present paper deals with new results obtained by direct numerical simulation in order to predict the kinematic dynamo effect inside the core of the reactor.

The core of a FBR seems to be favorable to the dynamo effect for several reasons (part II): 1) the flow inside the core possesses a strong helicity; 2) the magnetic Reynolds number at the scale of the core is larger than 10; 3) some ferromagnetic elements inside the core may disturb the phenomena because of their high magnetic permeability ($10^3\mu_0$); and 4) the core is surrounded by a ferromagnetic crown that may act in favor of the dynamo effect.[5]

The complexity of the flow frontiers, the extended spatial scale of the flow geometry (three decades), an approximated knowledge of the turbulent flow in the core, and the heterogeneousness of the magnetic properties of the materials are the main difficulties to face. The time evolution of magnetic induction B is given by

$$\partial \boldsymbol{B}/\partial t = \mathrm{rot}(\boldsymbol{V} \times \boldsymbol{B}) + R_m^{-1}\nabla^2 \boldsymbol{B} \qquad (1)$$

Dynamo effect is reached unless $B(t) \to 0$ when $t \to \infty$.

The nonsymmetric distribution of the ferromagnetic elements within the core leads to a heavy modeling (three-dimensional and unstationary) of Eq. (1) by the finite element method (Part III). Two cases have been simulated. The first one (Part IV) is treating the case of a homogeneous core (without any ferromagnetic elements). The second one (Part V) is treating the case of a heterogeneous core (with 10% of ferromagnetic elements).

II. Hypothesis

The following hypotheses are concerning the FBR Phenix.

A. Fast Breeder Reactor Geometry

The reactor is composed of two sodium loops (Fig. 1). The primary loop is contained in a tank (1) with the sodium motion being forced by three pumps (2). The sodium is heated inside the core (4) and gives its heat to the secondary loop (6) through three primary heat exchangers (5). The sodium motion of the secondary loop (6) is forced by three pumps (7). It gives its heat to water loops (9) through secondary exchangers (8).

B. Fast Breeder Reactor Core Geometry

The FBR's core is composed of three main parts (Fig. 2): the lateral neutronic protection made of ferromagnetic materials, the outer core where the motion of sodium is slow, and the inner core that has the following characteristics: mean axial velocity of the sodium in the inner core, $V_0 = 5$ m/s $-$ 1; mean flow rate, $Q = 3.7$ m^{-3}/s^{-1}; efficient radius of the core, $(Q/\pi V_0)^{0.5} = 0.5$ m; mean electrical conductivity (temperature between 400 and 560°C), $\sigma = 4.1\ 10^6 \Omega^{-1}\mathrm{m}^{-1}$; and magnetic permeability of nonferromagnetic elements, $\mu_0 = 4\pi\ 10^{-7}$H m^{-1}.

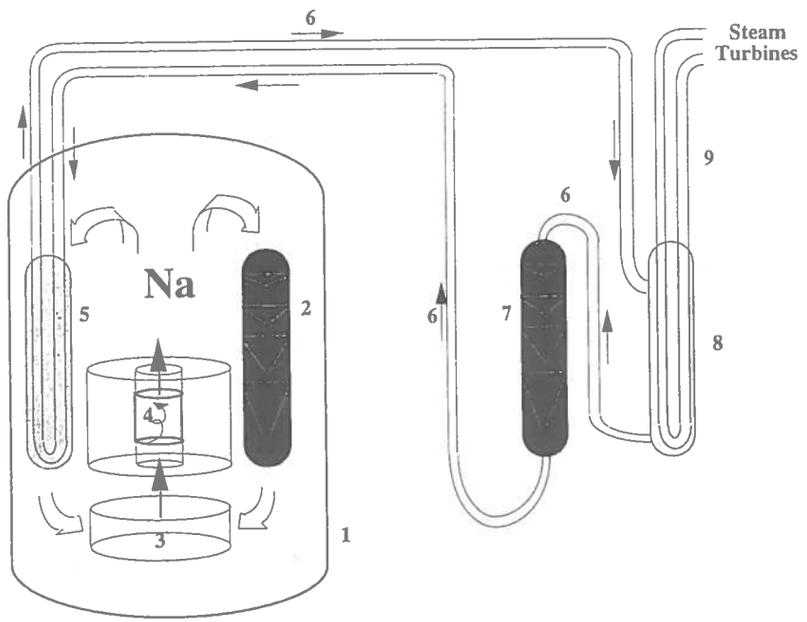

Fig. 1 Principal scheme of a compact type fast breeder reactor.

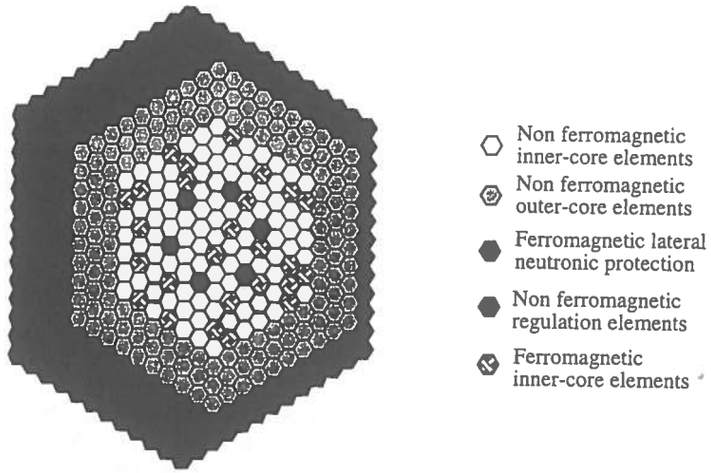

Fig. 2 Horizontal section of the Phenix reactor.

These values lead to the following magnetic Reynolds number:

$$R_m = \sigma\mu_0 V_0 (Q/\pi V_0)^{0.5} = 13 \tag{2}$$

which is high enough to generate some eventual dynamo effect.

The inner core is composed of about a hundred cylindrical elements of the hexagonal section. It is then obvious that the magnetic Reynolds number at the scale of each element should be lower than one and then unable to generate dynamo effect. However, the sodium motion in each element is guided by 217 helical space wires for optimal thermal exchange reasons. This action leads to a local azimuthal component of the velocity field with a double effect: the increase of the magnetic Reynolds number to a value close to one (for the same axial flowrate), and a nonzero helicity value of the motion, which is known to act in favor of a dynamo.[7]

C. Core's Flow Model

One of the difficulties of the numerical modeling of the kinematic dynamo comes from the necessity to introduce a sufficiently simple model of the motion in each hexagonal element, keeping nonetheless the characteristics essential to the appearance of the phenomena: magnetic Reynolds number and helicity. The simplified model of the velocity field that is presented in the following is based on a previous study offering experimental and numerical results.[8] The mean flow rate and the mean helicity in each element have been computed on the basis of these results and reported in

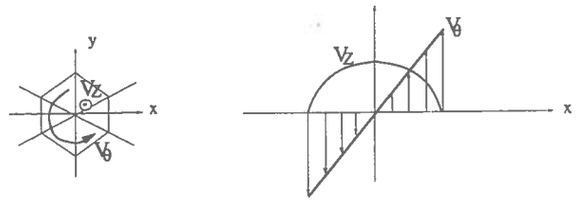

Fig. 3 Velocity field in one hexagonal element (horizontal section).

the following velocity model (Fig. 3). In each hexagonal element of symmetry axis $r = r_0$, the velocity field is defined in Cartesian coordinates by

$$V_x = -(y - y_0)\omega \tag{3a}$$

$$V_y = +(x - x_0)\omega \tag{3b}$$

$$V_z = 2V_0 \{1 - [(x - x_0)^2 + (y - y_0)^2]/R_2\} \tag{3c}$$

with $\omega = 100$ rad/s^{-1} and $V_0 = 1.8$ m/s^{-1}.

D. Electromagnetic Properties

The walls of 10% of the inner core elements are made with ferromagnetic materials (Fig. 2). Their magnetic permeability is 10^3 times larger than the rest of the core. A computation based on magnetostatic assumptions[9] leads to a magnetic interaction rate between the inside and the outside of each ferromagnetic element lower than 4%.* Thus the ferromagnetic wall is actually acting as a magnetic screening strongly limiting the interactions between the inner element and the outer element. As the local magnetic Reynolds number is too low to lead to magnetic self-excitation (around 1), the role of the sodium motion in each ferromagnetic element is considered as insignificant for dynamo action. Therefore, each one of them is replaced by a full ferromagnetic hexagonal cylinder with no velocity inside (Fig. 4).

The lateral neutronic protection (Fig. 2) is made of ferromagnetic material. Its presence is modeled by a homogeneous Neuman frontier condition on potential vector A. This implies a magnetic field direction normal to the frontier.

*Let us consider, for example, an outer current density creating an outer magnetic field. Then, a part of this magnetic field can penetrate into the wall and also into the inner element. If the magnetic permeability of the wall is equal to 10^3, then the intensity of the inner element penetrating the magnetic field is lower than 4% of the outer magnetic field.

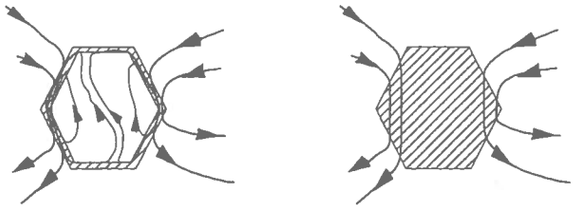

Fig. 4 Modeling of one hexagonal element with its ferromagnetic wall. The latter is acting as a magnetic screening between the inside and the outside of the element.

III. Numerical Model

A. (*A*, *W*) Modeling

Because of the complexity of the geometry, the number of nodes is very large (60,000). To be solved, the time-dependent linear system must not be ill-conditioned or nonsymmetric. Vector and electric potentials $\boldsymbol{A}$ and φ are found to be optimal unknowns on the spatial continuity point of view.[10] They verify the following system equivalent to Eq. (1):

$$\begin{cases} \operatorname{curl}\left(\dfrac{1}{\mu}\operatorname{curl} \boldsymbol{A}\right) = \sigma\left(-\dfrac{\partial \boldsymbol{A}}{\partial t} - \operatorname{grad}\varphi + \boldsymbol{V}\times\operatorname{curl}\boldsymbol{A}\right) \\ \operatorname{div}\sigma\left(-\dfrac{\partial \boldsymbol{A}}{\partial t} - \operatorname{grad}\varphi + \boldsymbol{V}\times\operatorname{curl}\boldsymbol{A}\right) = 0 \\ \operatorname{div}\boldsymbol{A} = 0 \end{cases} \tag{4}$$

the post-processing equations being given by

$$\boldsymbol{E} = -\operatorname{grad}\varphi - \frac{\partial \boldsymbol{A}}{\partial t}, \quad \boldsymbol{j} = \sigma\left(-\operatorname{grad}\varphi - \frac{\partial \boldsymbol{A}}{\partial t} + \boldsymbol{V}\times\operatorname{curl}\boldsymbol{A}\right),$$
$$\boldsymbol{B} = \operatorname{curl}\boldsymbol{A}, \quad \boldsymbol{H} = \frac{\operatorname{curl}\boldsymbol{A}}{\mu} \tag{5}$$

A classic finite element Galerkin projection of the first-order time-dependent finite difference scheme of Eq. (4) involves a nonsymmetric ill-conditioned system. The nonsymmetric part of the time-dependent matrix can be symmetrized introducing a new unknown W defined by[10]

$$\varphi = \frac{\partial W}{\partial t} \tag{6}$$

The ill-conditioned system given by the term $\operatorname{curl}(\mu^{-1}\operatorname{curl} A)$ can be mixed with the gage equation div A by a penalty method to obtain a Laplacian formulation. The weak form of Eq. (4) is then derived on the vectorial space of projection functions α_i, and scalar functions β_i:

$$\begin{cases} \displaystyle\iiint_{(\Omega)} \left\{\frac{1}{\mu}\operatorname{curl}\alpha_i\cdot\operatorname{curl}\boldsymbol{A} + (\text{penalty})\operatorname{div}\alpha_i\operatorname{div}\boldsymbol{A} \right. \\ \qquad \left. + \sigma\alpha_i\cdot\left(\dfrac{\partial(\boldsymbol{A}+\operatorname{grad}W)}{\partial t} - \boldsymbol{V}\times\operatorname{curl}\boldsymbol{A}\right)\right\} dV \\ \qquad - (\text{penalty}) \displaystyle\oiint_{(I)+(\Gamma)} \alpha_i\cdot\boldsymbol{n}\operatorname{div}\boldsymbol{A}\, dS + \oiint_{(I)+(\Gamma)} \alpha_i\cdot(\boldsymbol{n}\times\boldsymbol{H})\, dS = 0 \\ \displaystyle\iiint_{(\Omega)} \sigma\operatorname{grad}(\beta_i)\cdot\left(\frac{\partial(\boldsymbol{A}+\operatorname{grad}W)}{\partial t} - \boldsymbol{V}\times\operatorname{curl}\boldsymbol{A}\right) dV \\ \qquad + \displaystyle\oiint_{(I)+(\Gamma)} \beta_i\sigma\left(\frac{\partial(\boldsymbol{A}+\operatorname{grad}W)}{\partial t} + \boldsymbol{V}\times\operatorname{curl}\boldsymbol{A}\right)\cdot\boldsymbol{n}\, dS = 0 \end{cases} \tag{7}$$

The convective terms $\boldsymbol{V}\times\operatorname{curl}\boldsymbol{A}$, in reason of their dependence on V, cannot lead to a symmetric matrix. Then they must be rejected to the second member of the equations using an iterative process between them and the rest of the system. The resolution takes the following form:

$$(\Delta t M + L)X_i^{n+1} = LX^n + \Delta t F\left(X_{i-1}^{n+1}\right) \tag{8}$$

where $X_i^{n+1} = (A_x, A_z, W)$ at the time step $(n+1)\Delta t$ and at the ith iteration and X^n these values at the preceding time step. In this expression, $(\Delta t\, M + L)$ is symmetric and well-conditioned, and F is the quadri-vectorial function corresponding to the convenctive terms.

This formulation has been described with the Flux–Expert* generator package[11] with second order three dimension isoparametric curvilinear finite elements, and the linear systems are solved by incomplete Cholesky conjugate gradients iterative algorithm (see Ref. 12 for more details).

B. Stability

To describe time dependence, an implicit first-order finite differences algorithm is used. As the implicit method is unconditionally stable, there is no stability constraint on time-step size.

To treat a spatial derivative of the convective terms, a central difference scheme is used rather than an upwind scheme. The reason for this choice is

*FLUX-EXPERT is a registered trademark from DT21 S.A., 8 chemin dees Pèles 38240 Meylan, France.

to avoid adding numerical attenuation to the physical instability when evidence is searched. Therefore the following relation must be fullfilled on each mesh element of the domain:

$$(R_m)_{\text{mesh element}} < 2 \tag{9}$$

where $R_m = \sigma\mu VL$ with V and L being the characteristic velocity and dimension of the mesh element.

C. Precision

The time step is adjusted so that it is smaller in each mesh element than the convection and diffusion characteristic times. Indeed, these mechanisms are essential for the dynamo effect. As $(\Delta t)_{\text{diff}} = \sigma\mu(\Delta x)^2$ and $(\Delta t)_{\text{conv}} = \Delta_x V^{-1}$,

$$\begin{cases} \text{if } (R_m)_{\text{mesh}} < 1, \text{ then } \Delta t < (R_m)_{\text{mesh}} \Delta x V^{-1} \\ \text{if } (R_m)_{\text{mesh}} > 1, \text{ then } \Delta t < \Delta x V^{-1} \end{cases} \tag{10}$$

At last, mesh size must be small enough to represent the largest variations of the unknowns without numerical rebound.

D. Preliminary Tests

Some preliminary tests showing good accuracy with previous analytical results have been done. A simulation of the 1988 Gailitis et al. experiment has been done for a magnetic Reynolds number equal to 19. The simulation was self-excited in conformity with the extrapolation of the experimental results.[13]

IV. Homogeneous Case

Several simulations have been done for a different number of hexagonal elements, from 1 to 61. For each one of them, the whole domain is homogeneous in terms of magnetic permeability and electrical conductivity without taking care of the ferromagnetic lateral neutronic protection. Outside the hexagonal elements the velocity field is equal to zero. Inside each element the velocity field is defined by Eqs. (3a–3c). The characteristics of the simulations are summarized in Table 1.

The main goal of these simulations is to evaluate the number of elements (each one containing a screw motion) necessary to obtain dynamo effect. This point is interesting from a fundamental point of view as an intermediate case between a single and an infinity of screw motions. Indeed, the single screw motion has been shown to self-excite above a critical magnetic Reynolds number of 17 for a body motion and 20 for a Couette–Poiseuille profile.[14,15] In the infinite case there always exists magnetic axial wave numbers that are self-excited depending on the magnetic Reynolds number.[6,16]

Table 1 Simulation parameters of the homogeneous and heterogeneous cases

Element radius, m	Domain radius, m	σ, $\Omega^{-1}m^{-1}$	μ_0, H m^{-1}	V_z, m s^{-1}	$\omega_{\max}$, rad/s^{-1}	Δt, s
0.06	2	4.10^6	$4\pi 10^{-7}$	3.6	100	0.009

Another issue of these simulations is the evaluation of the critical size of an FBR core above which self-excitation may occur. The French Superphenix reactor's core, for example, is composed of 364 hexagonal elements (instead of 103 for Phenix).

A. Magnetic Growth Rate in Function of the Number of Elements

On Fig. 5 the time evolution of magnetic energy is sketched for different numbers of elements. In each case the magnetic energy is decreasing, so that the dynamo effect is not reached. Nevertheless, the decrease is less strong when the number of elements is larger. Therefore one can expect that for a sufficiently large number of elements, the dynamo can be reached. An extrapolation of the results is shown in Fig. 6 displaying the number of elements in the function of the growth rate. A zero value of the latter is obtained for a number of elements varying between 300 and 900 depending on the extrapolation method (linear or quadratic) that is used. To avoid this extrapolation lack of precision, the best idea would be to raise the number

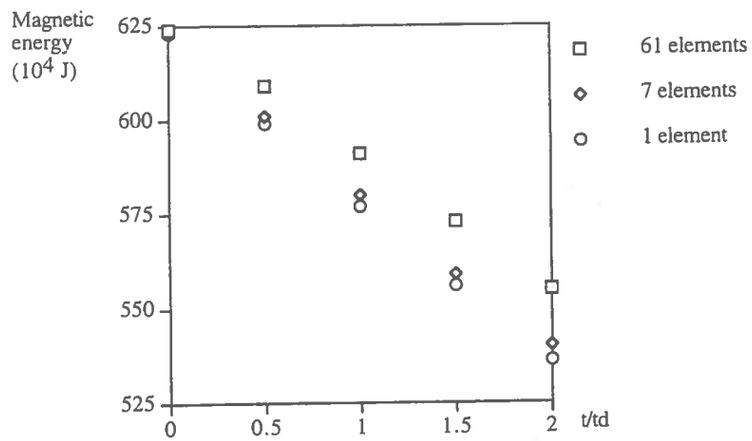

Fig. 5 Magnetic energy in function of adimensional time t/t_d for different numbers of elements. The diffusion time t_d is calculated on the basis of one element radius R: $t_d = \sigma\mu_0 R^2 = 0.09$ s.

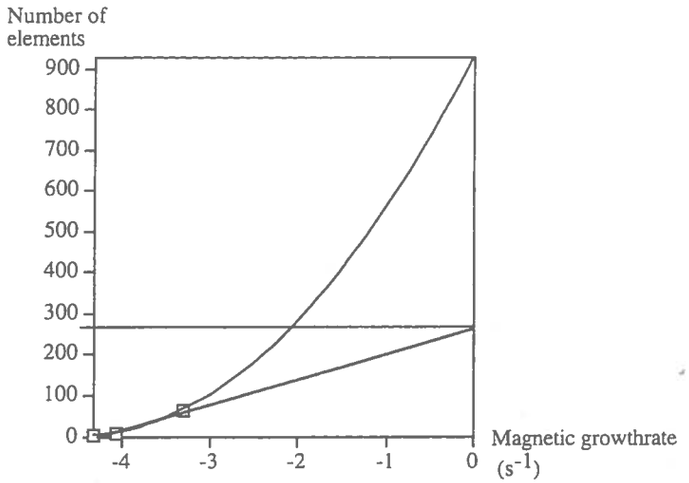

Fig. 6 Extrapolation of the minimum number of elements needed to obtain a positive growth rate of magnetic energy E. The latter is evaluated by the Lyapunov exponent: $t^{-1}\ell nE$.

of elements within the direct simulation. This is difficult, however, because of the computer's limitations. In the 61 elements case, for example, computation on a Cray C94 Vectorial computer lasted about 10 for each time step. Nevertheless, these results show that the FBR Phenix is subcritical in the case of homogeneous core.

B. Simulation of 61 Elements

At the initial time ($t = 0$), $B_z = 0$ and a nonzero horizontal initial magnetic field is given with a variation scale equal to the core's size. As the motion scale is equal to one element's size, one could expect that the vertical component B_z induced by the motion would also be at the scale of one element's size. Figure 7 shows that it is actually the case. But, a large scale B_z is also taking place (Fig. 7), probably resulting from an inverse cascade generation process.[17]

V. Heterogeneous Case

On the basis of the assumptions summarized in Section II, a realistic simulation of the Phenix FBR's core has been done. All of the different regions (Fig. 2) have been represented. However, because of the limited computer machine capacity, only 91 elements have been modeled instead of 127 in reality. To keep the preconditionment of the resolution system healthy the permeability of the ferromagnetic elements is taken equal to $10^2\mu_0$ instead of $10^3\mu_0$. This action can affect the result in the way of an underesti-

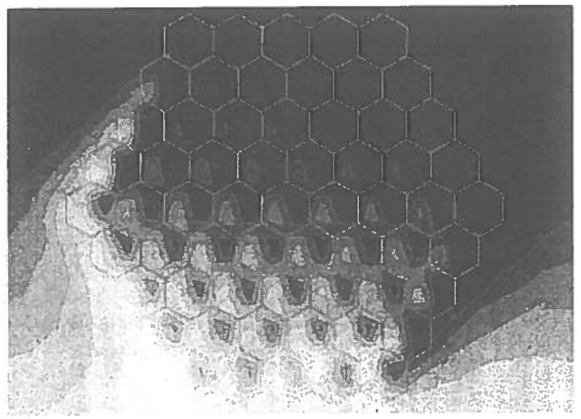

Fig. 7 Isovalues of the magnetic field axial component B_z in a horizontal section. From dark to light, negative to positive values of B_z. B_z is present at the scale of each hexagonal element and also at the scale of the core.

mation of the dynamo effect probability. The other characteristics of the simulation are identical to the previous homogeneous case (Table 1).

A. Growth Rate Within Different Regions of the Core

On Fig. 8, the time evolution of magnetic energy is sketched for different regions of spatial integration of the magnetic energy density $B^2/s2\mu$. In any nonferromagnetic region the magnetic energy is decreasing along the time. Then, the dynamo effect is not obtained at the scale of the FBR's core. Nevertheless, inside the ferromagnetic elements the magnetic energy is strongly increasing. The corresponding growth rate is very strong (around 40 s^{-1}) compared to the decrease in the other regions ($-6\ s^{-1}$), possibly leading quickly to a large value of the magnetic field.

B. Magnetic Field Repartition

As expected by the magnetostatic theory (Section II.D), the magnetic field lines are concentrated on the periphery of the ferromagnetic elements (Fig. 9). Its intensity is growing inside the ferromagnetic elements and decreasing outside.

VI. Discussion

Maybe the most important question concerning the preceding results is to know if the growth of the magnetic energy within the ferromagnetic elements comes from a real dynamo effect. The question is difficult to answer because even if the computation time is twice the characteristic diffusion time inside a nonferromagnetic element, then it is nonetheless only a little

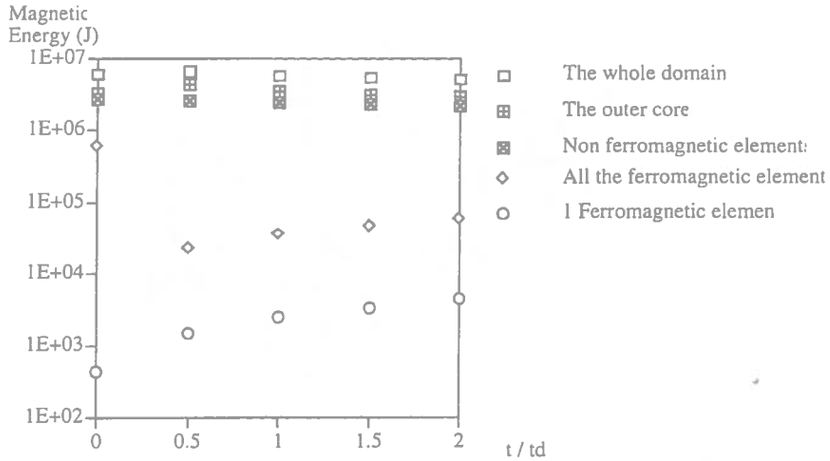

Fig. 8 Magnetic energy in function of adimensional time t/t_d in the presence of ferromagnetic elements. The different curves are corresponding to different regions of the domain on which the magnetic energy has been computed. The diffusion time t_d is calculated on the basis of one nonferromagnetic element $t_d = \sigma\mu_0 R^2 = 0.09$ s.

fraction of the characteristic diffusion time of a ferromagnetic element. Thus, seemingly if one could increase the number of time steps at least by a factor of 100, then possibly one could know if the phenomena are only the result of a convective transient state or if the magnetic field will be increas-

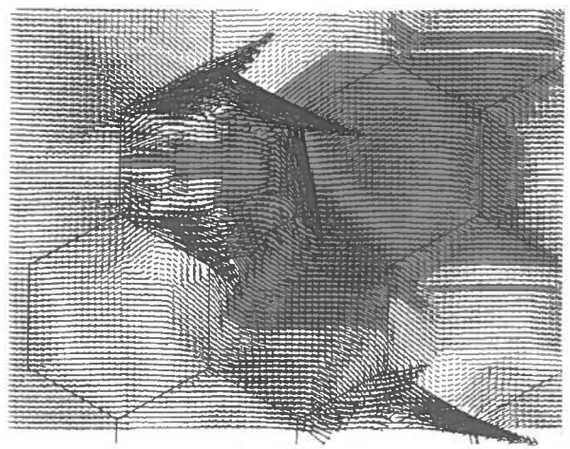

Fig. 9 Horizontal magnetic field in a horizontal section around a ferromagnetic hexagonal element.

ing in all of the domains by a dynamo effect. A definitive answer cannot be given with the present model as the computation time needed for four time steps is already very large (40H of Vectorial Cray computer). However, the opportunity of doing such computations must be possible on parallel and high parallel Cray computers. The present model is now being reprogrammed to be able to run on such computers.

For the FBR authorities the previous results are yet very important. Indeed, even if the magnetic field increase is only a convective transient state, then the increase can still occur during the functioning of the reactor. This sudden increase is probably dependent on the initial magnetic conditions. Suppose that at a certain time the initial conditions are favorable, then the strong amplification of the magnetic field will be accompanied by a growth of the electromagnetic forces. The latter can then lead to eventual large strains on the element's structure, which is not desirable.

Acknowledgment

F. P. was supported by the fast breeder reactor Phenix under Contract 5061 3A099450.

References

[1]Bevir, M. K., "Possibility of Electromagnetic Self-Excitation in Liquid Metal Flows in Fast Reactors," *Journal of the British Nuclear Engineering Society*, Vol. 12, No. 4, 1973, pp. 455–458.

[2]Kirko, G. E., "Phénomènes Électromagnétiques Dans les Grandes Masses de Métaux Liquides," trad. CEA No. 2.722.1, 1984.

[3]Garnier, J., "Synthèse et Critique des Travaux de l'Académie des Sciences Soviètique Concernant les Effects Thermoelectromagnetohydrodynamiques Dans les Surgénérateurs," Tech. Note NR, 1986.

[4]Alemany, A., and Marty, Ph., "L'étude des Perturbations Magnétiques au Voisinage des Pompes Secondaires de Superphénix," 1rst rapport INPG-LEGI/EDF-CLI, 1995.

[5]Marty, Ph., Ajakh, A., and Thess, A., "Magnetic Fields in Fast Breeder Reactors: New Results on Thermoelectricity and Dynamo Effect," *Magnetohydrodynamics*, Vol. 30, No. 4, 1994.

[6]Plunian, F., Alemany, A., and Marty, P., "Influence of Magnetohydrodynamic Parameters on Electromagnetic Self-Excitation in the Core of a Fast Breeder Reactor," *Magnetohydrodynamics* (to be published).

[7]Léorat, J., Pouquet, A., and Frisch, U., "Fully Developed MHD Turbulence Near Critical Magnetic Reynolds Number," *Journal of Fluid Mechanics*, Vol. 104, 1981, pp. 419–443.

[8]Lafay, J., Menant, B., and Barroil, J., "Local Pressure Measurements and Peripherical Flow Visualization in a Water 19-Rod Bundle Compared with FLICA II B Calculations: Influenced of Helical Wire-Wrap Spacer System," ASME, Aug. 1975.

[9]Durand, E., *Magnétostatique*, Masson and Cie, 1968.

[10]Biro, O., and Kurt, P., "On the Use of the Magnetic Vector Potential in the Finite

Element Analysis of Three-Dimensional Eddy Currents," *IEEE Transactions on Mag.*, Vol. 25, No. 4, 1989.

[11]Massé, Ph., "Modeling of Continuous Media Methodology and Computer-Aided Design of Finite Element Programs," *IEEE Transactions on Mag.*, Vol. 20, No. 5, 1984, pp. 1885–1890.

[12]Plunian, F., and Massé, Ph., "An Optimal Preconditioned Scheme for FE Modelization of Kinematic MHD Dynamo Effect," *Proceedings of Ecomas96* (to be published).

[13]Plunian, F., Alemany, A., Marty, Ph., and Massé, Ph., "A Finite Element Modeling of the 1988 Gailitis et al MHD Dynamo Experiment," *Magnetohydrodynamics* (submitted for publication).

[14]Ponomarenko, Yu. B., "On the Theory of Hydromagnetic Dynamo," *Zh. Prikl. Mekh. Tekhn. Fiz.*, USSR, Vol. 6, 1973, pp. 47–51.

[15]Gailitis, A., Karasev, B. G., Kirillov, I. G., and Lielausis, O., and Ogorodnikov, A. P., "The Helical MHD Dynamo," *Proc IUTAM*, Riga, 1988.

[16]Roberts, G. O., "Dynamo Action of Fluid Motions with Two-Dimensionnal Periodicity," *Philosophical Transactions of the Royal Society of London*, Vol. A271 1972, p. 411.

[17]Frisch, U., Pouquet, A., Léorat, J., and Mazure, A., "Possibility of an Inverse Cascade of Magnetic Helicity in MHD Turbulence," *Journal of Fluid Mechanics*, Vol. 68, Pt. 4, 1975, pp. 769–778.

Chapter 36

Influence of Magnetic Field Inhomogeneity on the Operation of Magnetohydrodynamic Devices

A.V. Zagorskii*
Institute of Theoretical and Applied Mechanics, Novosibirsk, 630090, Russia

I. Introduction

WE WILL consider the operation of a magnetohydrodynamic device of the type of plasma driven electromagnetic rail accelerator, a railgun (Fig. 1), in which the acceleration is a result of the interaction between the current through the plasma and the magnetic field. The magnetic field can be created by the current-carrying rails as well as by a special outer source. A great number of works are devoted to the investigation of such accelerators.[1–5] The state of railgun plasma armature (PA) and the acceleration dynamics of the projectile are determined by the ratio of the accelerating force to the momentum losses connected with the turbulent friction and entrainment of a mass eroded off the channel walls. At the beginning of the process, the Lorentz force exceeds losses quite significantly. This result leads to a relatively small PA length (about several channel calibers) and a high acceleration rate. But as velocity and PA mass increase, the losses become comparable with the pushing force. As a result, acceleration stops, and the PA length drastically increases.

The system of equations describing the railgun operation in a quasi-one-dimensional approach is as follows:

$$\frac{\partial \rho}{\partial t} + \frac{\partial \rho u}{\partial x} = q_e$$

$$\rho \frac{\partial u}{\partial t} + \rho u \frac{\partial u}{\partial x} = -\frac{\partial p}{\partial x} + F_m - f_t - u q_e$$

*Senior Research Worker, Laboratory of Fast-Process Physics.